

# Nanoscale fluid-structure interaction: Flow resistance and energy transfer between water and carbon nanotubes

Chao Chen,<sup>1,2,3</sup> Ming Ma,<sup>1,2,3</sup> Kai Jin,<sup>1</sup> Jefferson Zhe Liu,<sup>4</sup> Luming Shen,<sup>3</sup> Quanshui Zheng,<sup>1,2</sup> and Zhiping Xu<sup>1,2,\*</sup>

<sup>1</sup>*Department of Engineering Mechanics, Tsinghua University, Beijing 100084, China*

<sup>2</sup>*Center for Nano and Micro Mechanics, Tsinghua University, Beijing 100084, China*

<sup>3</sup>*School of Civil Engineering, University of Sydney, Sydney, NSW 2006, Australia*

<sup>4</sup>*Department of Mechanical and Aerospace Engineering, Monash University, Clayton, Victoria 3800, Australia*

(Received 2 August 2011; published 18 October 2011)

We investigate here water flow passing a single-walled carbon nanotube (CNT), through analysis based on combined atomistic and continuum mechanics simulations. The relation between drag coefficient  $C_D$  and Reynolds number  $Re$  is obtained for a wide range of flow speed  $u$  from 5 to 600 m/s. The results suggest that Stokes law for creep flow works well for small Reynolds numbers up to 0.1 ( $u \approx 100$  m/s), and indicates a linear dependence between drag force and flow velocity. Significant deviation is observed at elevated  $Re$  values, which is discussed by considering the interfacial slippage, reduction of viscosity due to friction-induced local heating, and flow-induced structural vibration. We find that interfacial slippage has a limited contribution to the reduction of the resistance, and excitations of low-frequency vibration modes in the carbon nanotube play an important role in energy transfer between water and carbon nanotubes, especially at high flow speeds where drastic enhancement of the carbon nanotube vibration is observed. The results reported here reveal nanoscale fluid-structure interacting mechanisms, and lay the ground for rational design of nanofluidics and nanoelectromechanical devices operating in a fluidic environment.

DOI: [10.1103/PhysRevE.84.046314](https://doi.org/10.1103/PhysRevE.84.046314)

PACS number(s): 47.61.Fg, 62.25.-g, 83.50.Rp, 66.20.Cy

## I. INTRODUCTION

Recently there has been immense interest in utilizing functional nanostructures in electromechanical devices [1]. In these devices, deformation or vibrations of nanostructures are responsible for mechanical operations [2]. Electrochemical actuators, resonators with ultrahigh frequencies, and ultrasensitive biochemical and mass sensors that are able to detect tiny mass and biological molecules have been fabricated following this concept [3–5]. Remarkable qualities originate from both the intrinsic mechanical properties of nanostructures and their responses to environmental triggers. The interaction between a nanodevice and its environment is thus a key for its performance. For example, a strong coupling with viscous fluid could overdamp a vibrating nanobeam and turn a resonator into a relay [6]. On the other hand, in a nanofluidic device, manipulation and precise control of fluids are achieved under a spatial confinement at the molecular level. At this scale, interesting phenomena can arise from either atomistic discreteness of the nanostructure or its interface to the environmental fluid where it is immersed. Nevertheless, in contrast to macroscopic counterparts of the nanoelectromechanical or nanofluidic devices, where continuum dynamics works well, the atomistic mechanisms of the interplay between nanostructures and their fluid environments are not well understood in spite of their extreme importance in nanotechnology-enabled applications.

Fluid-structure interaction (FSI) is a crucial topic in the field of hydrodynamics that has been studied for a century since Stokes' work [7]. However, its mechanisms and physical significance at the molecular level have not been clarified yet. There are several issues where serious attention should be paid. Firstly, solvent molecules close to the solid wall feature

a different structure from the bulk phase due to the fluid-solid interface and cohesion. Secondly, interfacial slippage, friction, and the renormalization of viscosity from local temperature change could also lead to remarkable deviations in both the flow dynamics and mechanical energy transfer between fluid and solid from the classical hydrodynamics predictions [7–9]. At the nanoscale ( $l \approx 1$  nm), a water molecule moves at a speed close to its thermal velocity (on the order of 100 m/s at room temperature from the equipartition theorem); thus the timescale for one molecule to slide over a crystalline lattice reaches the order of picoseconds [8]. When a fluid flow with speeds in this range is driven on an atomistically smooth surface such as the inner wall of carbon nanotubes, a frictional force on the order of gigahertz is exerted to the nanostructure, which is on the same order as those for low-frequency phonon modes in typical nanostructures, such as the flexural and breathing modes of a carbon nanotube. Thus it is expected that a significant coupling (even a resonance) between the fluid and structure could occur, which is capable of modifying the water structure and drag force, and channeling significant kinetic energy from the fluid to structural vibration [9].

For a flow on the nanometer scale, the Reynolds number is usually very low ( $Re \sim 0.1$ , where  $Re = \rho u l \mu^{-1}$  and  $\rho$  and  $\mu$  are the density and dynamics viscosity of water at room temperature, respectively) according to the reduction of spatial dimension, even at a respectable flow rate ( $u = 10$ – $100$  m/s). At this low  $Re$  limit, the Stokes approximation for creep motion flow simplifies the Navier-Stokes equation. Dimensional analysis predicts

$$C_D = C/Re, \quad (1)$$

where a dimensionless drag coefficient  $C_D$  is defined as  $f/(S\rho u^2/2)$  and  $S$  is the frontal area facing the flow, where  $f$  is the drag force [10]. The parameter  $C$  depends on specific

\*Corresponding author: xuzp@tsinghua.edu.cn

geometry and spatial arrangement of obstacles. For a circular cylinder immersed in an infinite flow region, continuum fluid dynamics calculations give  $C = 4.467$ . However, despite its great success for a macroscopic flow, the validity of this prediction at nanoscale has not been verified. As mentioned previously, we focus here on several critical issues at this length scale including (1) significant slippage at the fluid-structure interface [11–13], (2) viscosity change due to local heating and the restructuring of solvent structures, and (3) flow-induced excitation of structural vibration (or low-frequency phonon modes) of the nanostructures with significant mechanical energy transfer. To clarify them, we perform molecular dynamics (MD) and computational fluid dynamics (CFD) simulations for water flow around a single-walled carbon nanotube. MD simulations provide molecular level details, while in CFD simulations, the slipping boundary condition can be tuned empirically to investigate its effects.

## II. MODEL AND METHODS

### A. Molecular dynamics simulations

Carbon nanotubes are widely used in nanoscale electromechanical devices and nanofluidics, for their outstanding stiffness and electronic properties. Their perfect hexagonal graphene lattice and high rigidity lead to a slip length on the order of up to 100 nm for a flow along the axis, while slip length is  $< 1$  nm for a flow in the perpendicular direction [11,13]. Our MD simulations adopted the “Large-scale Atomic/Molecular Massively Parallel Simulator” (LAMMPS) package [14]. A single-walled armchair (5, 5) carbon nanotube (CNT) with a diameter  $d = 0.68$  nm and length  $l_{\text{CNT}}$  varying from 5 to 20 nm is immersed in a water box. An extended simple-point-charge (SPCE) water model is used to describe the water molecules [15–18]. The viscosity calculated from this model at room temperature is 0.729 mPa s. For comparison, we also apply a transferable intermolecular potential three-point (TIP3P) water model, which yields a viscosity of 0.321 mPa s at room temperature [16–19]. A Dreiding force field is used for carbon nanotubes including the  $sp^2$  carbon-carbon interactions and their interactions with the water molecules [20]. This force field is fitted to experimental lattice parameters, elastic constants, and phonon frequencies of graphite. Thus it is able to predict both elastic and vibrational behavior of carbon nanostructures, such as an experimentally consistent Young’s

modulus of 1.06 TPa for a (5, 5) carbon nanotube, when the thickness of a graphene sheet  $t = 0.34$  nm is used [21].

The van der Waals interaction between the carbon nanotube and water molecules is described by using a Lennard-Jones (LJ) potential  $E_{\text{LJ}} = 4\epsilon[(\sigma/r)^{12} - (\sigma/r)^6]$  between carbon and oxygen atoms. The LJ potential parameters define the contact angle  $\theta_{\text{CA}}$  of water over graphene. By fitting to the experimentally measured value for  $\theta_{\text{CA}}$ , although the modification of carbon-oxygen interactions by the curvature of the carbon nanotube walls is not taken into account, this model is expected to correctly predict the interaction and energy transfer between water and carbon nanotubes. We carried out MD simulations to determine the contact angles of a set of LJ parameters for both SPCE and TIP3P models, using the same technique as introduced in Ref. [22]. The results are summarized in Table I. In our following simulations, parameters corresponding to a contact angle of  $95.3^\circ$  are used if not specifically noted.

To drive a water flow around carbon nanotubes, a “gravity” body force  $f_g$  is applied on each water molecule perpendicular to the tube axis to simulate a pressure drop commonly applied in experiments [23]. From a hydrodynamics point of view,  $f_g$  contributes to the flow equally as a pressure drop; however, it is more convenient to implement a body force in MD simulations. The flow velocity field often converges after a transient period of  $\sim 50$  ps with an in-flow (out-flow) speed  $u$  ranging from 5 to 600 m/s, depending on the magnitude of  $f_g$ . Under such a steady state,  $f_g$  balances the friction force. At low speeds ( $u < 30$  m/s), the fluctuation is significant and a long-time simulation of the steady state is required for a reliable statistics of flow velocities and drag force. We evaluate the velocity field  $u(x, y)$  and drag force  $f$  by averaging over 1 ns simulations after steady state is reached.

Our molecular system is initially equilibrated at a specific temperature  $T = 300$  K and a pressure  $P = 1$  bar, by applying a Nosé-Hoover thermostat and barostat to water molecules for 300 ps. Then we switch to a  $NVT$  ensemble and drive the flow. The temperature of the flow is maintained by applying a thermostat after removing the center of mass drift motion to minimize thermostat disturbance. The carbon nanotube is allowed to deform with its center of mass motion being fixed during the simulation. Simulations with rigid carbon nanotubes, i.e., all carbon atoms are fixed in position, are also performed to investigate the effect of energy transfer between the flow and vibration of carbon nanotubes, which is neglected in an earlier work calculating the drag forces [11].

TABLE I. Lennard-Jones parameters for interactions between carbon and oxygen atoms.

| Water-CNT interaction | $\sigma$ (nm) | $\epsilon$ (meV) | Contact angle (deg) in Ref. [14] for SPCE model | Contact angle (deg) we measured for SPCE model | Contact angle (deg) we measured for TIP3P model |
|-----------------------|---------------|------------------|---|--|---|
| Model I               | 0.319         | 6.498            | 29.4  |  |   |
| Model II              | 0.319         | 5.8484           | 50.7  | 63.6   | 41  |
| Model III             | 0.319         | 4.5488           | 81.1  |  |   |
| Model IV              | 0.319         | 4.0626           | 95.3  | 99.6   | 90  |
| Model V               | 0.319         | 3.249            | 107.7   |  |   |
| Model VI              | 0.319         | 2.599            | 127.8   |  |   |
| Model VII             | 0.319         | 1.9495           | 143.3   | 137.9  | 139   |

Periodic boundary conditions are applied to all three directions with dimensions  $l_x = 4$  nm,  $l_y = 4$  nm, and  $l_z = l_{\text{CNT}} = 5$  nm, which yields equivalently a carbon nanotube array with a plane density of  $0.0625$  nm<sup>-2</sup>. To assure the simulation box is large enough and perturbation of the finite-size effects is negligible, we perform convergence tests with respect to the dimensions of the box perpendicular to the nanotube axis ( $z$  direction). The results show that a box with  $l_x$  and  $l_y$  larger than 4 nm gives a well-converged flow velocity field and resistance.

**B. Computational fluid dynamics simulations**

We perform finite element simulations to solve the Navier-Stokes equations. The interface between water and carbon nanotube is treated using a Navier slip boundary condition  $u_s = l_s \partial u_t / \partial n$ , where  $u_s$  is slip velocity,  $u_t$  is tangential velocity near the interface,  $n$  is the coordinate along normal direction of the surface, and  $l_s$  is Navier slip length that characterizes the slippage. Simulations are performed with an identical geometry as the MD simulations in a periodical flow region, which actually represents a rectangle carbon nanotube array separated by distances of  $l_x$  and  $l_y$ . A static circular cylinder represents a carbon nanotube across the  $z$  dimension of the box. The water flow is controlled by defining in-flow and out-flow speeds  $u$  ranging from 5 to 600 m/s. We set the viscosity here  $\mu = 0.729$  mPa s consistent with the SPCE model in our MD simulations. The carbon nanotube is considered as a rigid cylindrical boundary. The vibrational effect of carbon nanotubes is neglected. In our simulations, we investigate slip lengths from zero to a relative large value  $l_s = 1$   $\mu$ m, to cover its greatest possible range.

**III. RESULTS AND DISCUSSION**

**A. Resistance-flow rate relation**

With the previous definitions of drag coefficient  $C_D$  and Reynolds number  $Re$ , we illustrate their dependence in a logarithm diagram ( $\log_{10}$ ) for SPCE model calculations, as plotted in Fig. 1(a). It should be noted that the characteristic length scale, i.e., the diameter of a carbon nanotube, is calculated with respect to the midpoint between the first water molecule layer and the carbon atoms ( $l = 1$  nm), instead of the positions of carbon atoms, to evaluate  $C_D$  and  $Re$ . Figure 1(b) shows the drag force as a function of flow speed. The error bars represent the fluctuation when averaging over 1 ns after the steady states in our simulations.

From the simulation results we can see that for both the flexible and rigid nanotubes, when the flow speed  $u$  is below 100 m/s ( $Re < 0.1$ ), the dependence between  $f$  and  $u$  projects well into a scaling relation  $C_D = CRe^\alpha$ ,  $\alpha = -1.041$ , which is very close to the prediction from Stokes law  $\alpha = -1$  in Eq. (1). However, the coefficient  $C = 16.93$  is slightly higher as compared with the nonslip CFD simulation ( $C = 16.01$ ) in the  $\log_{10} C_D - \log_{10} Re$  plot [Fig. 1(a)]. This result, i.e.,  $\alpha \approx -1$ , indicates that the Stokes approximation for the low  $Re$  number flow is valid in the atomistic scale with corrections on the coefficient  $C$ .

When the speed  $u$  exceeds 100 m/s, a significant deviation from Stokes law is observed with a decreasing exponent  $\alpha$  in  $C_D = CRe^\alpha$  ( $\alpha < -1$ ), which indicates a reduced flow

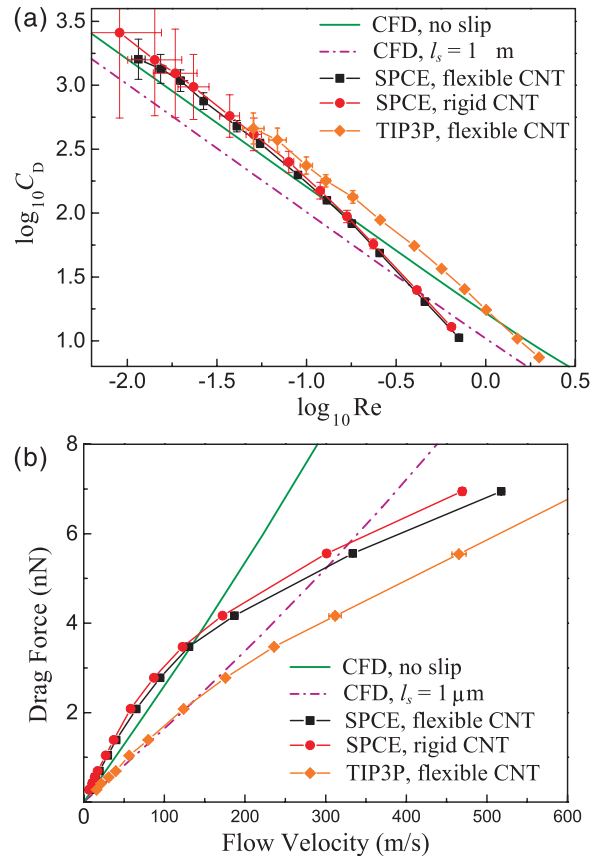


FIG. 1. (Color online) Flow resistance of water passing a (5, 5) carbon nanotube. (a) Results from molecular dynamics (MD) simulations (points with error bars for both velocity and force values) are compared with numerical results from Navier-Stokes equations (lines). In the computational fluid dynamics (CFD) simulations, we tune the slip length in the notion of the Navier boundary condition to account for the slip boundary conditions. The increasing of slip length results in downshift of  $\log_{10} C_D - \log_{10} Re$  curve. The CFD results fit well to a scaling function of  $C_D = CRe^{-1}$  in the entire range of  $Re$  values, while MD results deviate when the flow velocity exceeds  $Re = 0.1$  (SPCE) or  $Re = 0.3$  (TIP3P). (b) Dependence of drag force of the carbon nanotube on the flow velocity. The legends for forces are the same as in (a).

resistance as shown in Fig. 1(b). This trend appears in all our MD simulations. The reduction of exponent  $\alpha$  also indicates friction-induced heating at the interface while the flow speed is high. Besides, quantitative analysis shows that the flexibility of carbon nanotubes has limited effect on the drag force in our canonical ensemble MD simulations, which enhances as  $u$  increases [Fig. 1(b)].

In comparison, we also perform MD simulations using the TIP3P water model in a water flow around a flexible nanotube, with other settings maintained. The results are plotted in Figs. 1(a) and 1(b). There is a notable reduction of drag forces in comparison to the SPCE water model. This can be understood in terms of lower viscosity than that of SPCE model. Fitting the results by  $C_D = CRe^\alpha$  below  $Re < 0.3$  yields  $\alpha = -1.0196$  and  $C = 21.8$ . The linear hydrodynamics theory, i.e., the Stokes law, applies in both cases at low  $Re$  despite the very different viscosities. The transition point where the

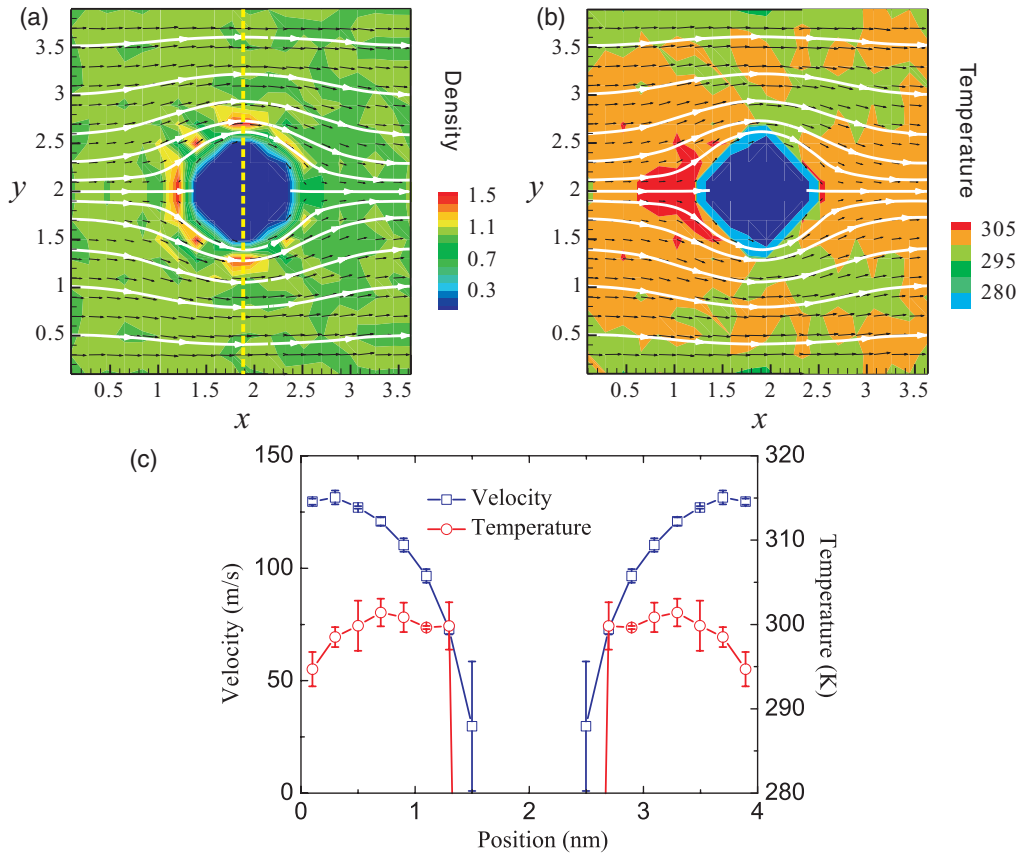


FIG. 2. (Color online) (a) Density and (b) temperature distribution across the  $x$ - $y$  plane (nanotube cross section). Local flow velocity field is plotted using arrowed lines. (c) Local flow velocity along the  $x$  direction and temperature as recorded along the dashed line in (a).

flow-resistance relation deviates from linear behavior is around  $u \sim 100$  m/s [Fig. 1(b)].

**B. Boundary slippage at the water-carbon nanotube interface**

For water flow around a flexible nanotube at 300 K, using the SPCE model, we plot a typical distribution of flow velocity, mass density, and temperature in Figs. 2(a) and 2(b). We observe a laminar flow pattern where the velocity converges to the horizontal direction in the far field. The velocity profile in the midplane [Fig. 2(c)] shows a significant interfacial slippage at the wall of the carbon nanotube, corresponding to a slip length on the order of 1 nm according to Navier’s definition. For carbon nanotubes and other graphene-related structures, there is a wide range for the slip length  $l_s$  reported in simulations and experiments, from nanometers to micrometers [8,11,13,24,25].

To understand how the interfacial slip affects the flow resistance, we perform CFD simulations with the Navier boundary condition, where slip length  $l_s$  is empirically tuned. In comparison with the one from MD simulation results, the scaling relation between  $C_D$  and  $Re$  from CFD simulation is well maintained in the  $Re$  range studied here. Figure 3 shows the reduction of drag force when interfacial slippage is considered. It is observed that drag force is reduced significantly when  $l_s$  is smaller than or comparable with the size of carbon nanotube. However, when  $l_s$  increases to more than four times the nanotube’s diameter, the drag force converges to a constant. Even

when the slip length reaches  $1 \mu\text{m}$ , the drag force reduces by only 14%, which corresponds to a downshift of the  $\log_{10}C_D$ – $\log_{10}Re$  curve by  $\sim 0.5$  in Fig. 1(a). In our MD simulations, a slip length is estimated to be on the order of 1 nm [Fig. 2(c)], thus the amount of drag force reduction must be quite limited. The deviation at elevated Reynolds numbers should come from

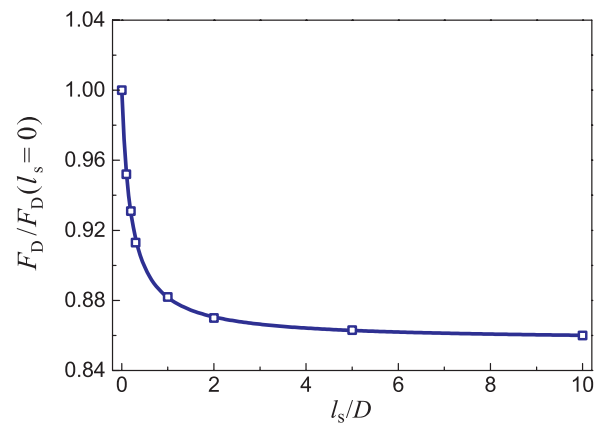


FIG. 3. (Color online) The effect of interfacial slippage on flow resistance. When the slip length  $l_s$  is smaller than or comparable to the size of carbon nanotube  $D$ , drag force  $F_D$  decreases significantly. However, when  $l_s$  increases further, drag force converges to a constant, and the overall reduction of  $F_D$  is limited by 14%.  $F_D$  with a nonslip boundary, i.e.,  $l_s = 0$ , is used as reference.

the local structure change of the water and the atomistic events occurring at the water-carbon nanotube interface.

This weak effect of slip length on the flow around carbon nanotubes is different from the flow inside carbon nanotubes. With a spatial confinement in carbon nanotubes, the giant slip length-to-tube diameter ratio leads to a remarkable increase of fluid flow rates: four to five orders of magnitude higher than the macroscopic Poiseuille flow [8,26]. This minor impact to the flow resistance suggests that the form drag from viscous pressure dominates here instead of skin friction drag.

**C. Fluid-structure interaction**

As shown in Fig. 1, above  $u = 100$  m/s, a clear deviation from both the scaling-law-based estimation  $Re^{-1}$  and CFD results is observed in our simulation results. One possible origin of this deviation is the change of local water structure and properties which cannot be captured in CFD. This change comes from flow-induced local heating of water molecules around the carbon nanotube, as shown in Figs. 2(b) and 2(c). Although coupled globally to a thermostat at  $T = 300$  K, the water molecules close to the carbon nanotube still have a much higher temperature than those in other regions, especially in the in-flow side of the carbon nanotube. The rise of local temperature reduces the viscosity of water. To quantitatively determine the local heating effect we perform a set of simulations at different temperatures. With the same external force applied, flow rates vary with the temperature of fluid. We use the viscosity value 0.729 mPa s of a SPCE model at room temperature as a reference to calculate the relative viscosity at other temperatures, as summarized in Fig. 4. The reduction of water viscosity due to local heating can reach more than 50% as the temperature rises from 278 to 338 K. Exponential fitting to the discrete MD results agrees with the theoretical prediction such as the exponential model  $\mu \propto \exp(-k_B T)$ . An equilibrium molecular dynamics simulation using the Green-Kubo formula also shows that the shear viscosity of water can be reduced by one order when the temperature increases from 273 to 373 K [19]. This heating effect can be further magnified

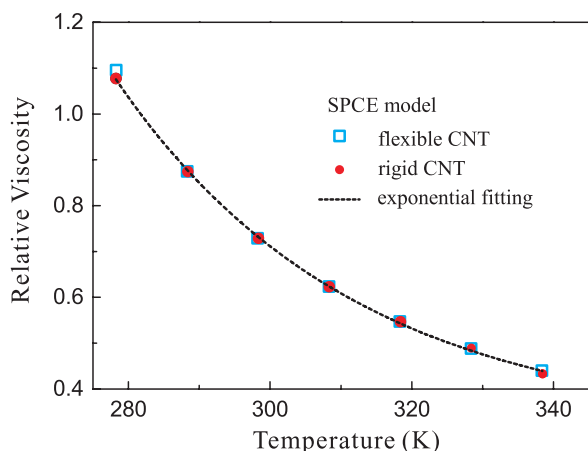


FIG. 4. (Color online) Thermal effect on the viscosity calculated using SPCE model. Results from water flow around both flexible and rigid nanotubes are plotted and fitted by an exponential function. The relative viscosity is compared with corresponding viscosity at 300 K for flexible and rigid CNTs, respectively.

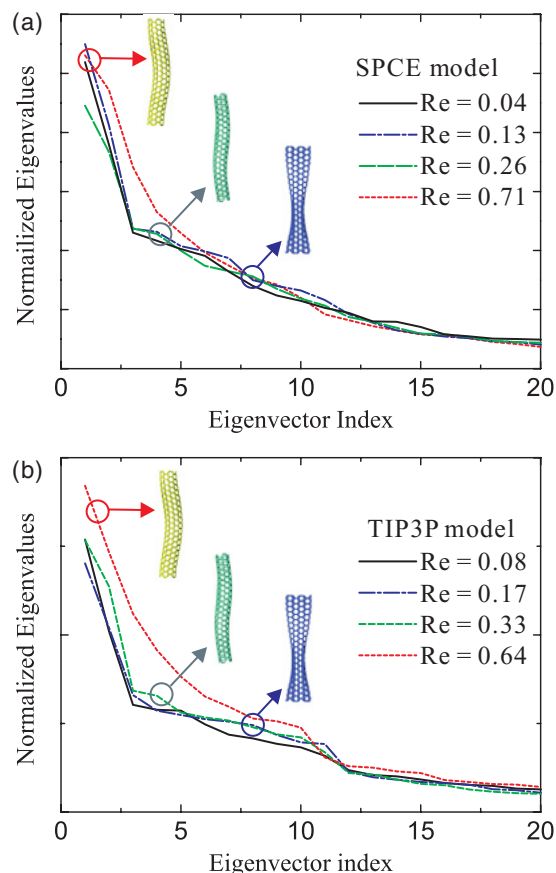


FIG. 5. (Color online) Vibrational modes excited by fluid flow, obtained as eigenvectors from principal component analysis, for both (a) SPCE and (b) TIP3P water models. The analysis indicates that as flow velocity increases, more and more modes with higher frequencies are excited. Specifically, when it exceeds 100 m/s, a significantly enhanced occupation of bending and breathing modes is observed, suggesting significant mechanical energy imported from water flow.

with enhanced fluid-structure interaction at higher speeds, which should be taken into account in the design of carbon nanotube-based devices operating in flow environments.

To gain further insight into the excitation of structural vibration in the carbon nanotube, principal component analysis (PCA) [9,27] is performed for the atomic trajectory  $\mathbf{x}_i(t)$ ,  $i = 1, \dots, 3N$ , for the first 500 ps, where  $N$  is the total number of atoms. Eigenvalues of the covariance matrix  $C_{ij} = \langle (\mathbf{x}_i - \langle \mathbf{x}_i \rangle)(\mathbf{x}_j - \langle \mathbf{x}_j \rangle) \rangle$  measure contributions of corresponding principal modes, where  $\langle \dots \rangle$  denotes the time average. The eigenmodes are thus translational, rotational, and vibrational modes. The results of PCA are shown in Fig. 5. As we can see, for both SPCE and TIP3P models, the most occupied vibrational modes as excited by the flow are beamlike bending modes, breathing modes, and the modes coupling these two. By comparing the PCA results from simulations under different flow speeds, we find that as the flow speed increases, more and more modes with higher frequencies are excited and a large amount of energy is pumped into the carbon nanotube from water flow. Specifically, when it exceeds 100 m/s, a significantly enhanced occupation of bending and breathing modes is observed, in consistence with what we have observed in the simulation trajectory. These results clearly indicate an energy

transfer process from flow field to the immersed carbon nanotubes.

The most activated modes we observe in the PCA analysis are the phonon modes of the carbon nanotube with the lowest frequencies which thus interact most significantly with the water molecules sliding around [28]. Moreover they could be tuned through selecting the nanotubes with specific radius  $r$ , length  $l_{\text{CNT}}$ , or using multiwalled carbon nanotubes. As an example, the frequency of the radial breathing mode is inversely proportional to the radius [29], and the frequency of the bending mode is

$$\omega = \frac{\beta^2}{l^2} \sqrt{\frac{EI}{\rho A}}, \quad (2)$$

where  $\beta$  is a numeric factor determined from the boundary conditions,  $E$  is the Young's modulus,  $I$  is the bending moment of inertia, and  $\rho$  and  $A$  are the mass density and cross-section area, respectively [30]. For our system, the frequencies of these modes are on the order of  $10^{12}$  Hz. Since the sliding events of water molecules ( $u \approx 100$  m/s) on the graphene lattice ( $a \approx 0.1$  nm) induce periodic perturbations with the frequency on the order of  $u/a \approx 10^{12}$  Hz, a strong vibrational coupling occurs, which leads to remarkable mechanical energy transfer

from water to the phonon modes of the carbon nanotube as mentioned [9,31,32].

#### D. Interface engineering

With the advantage of atomistic representation in the MD simulations, we also look directly into the roles of adhesive strength between water and carbon nanotube. We first tune the Lennard-Jones parameters between carbon and oxygen atoms in a range corresponding to a contact angle of water droplet on a single graphene sheet from  $30^\circ$  to  $140^\circ$ . Detailed parameters are listed in Table I [12]. The results shown in Fig. 6 indicate that  $\varepsilon$  directly defines the water structures close to the carbon nanotube, which in turn modifies the flow velocity field at a specific load. For  $\varepsilon = 1.9495$  meV instead of 4.063 meV, the water molecules near the carbon nanotube are less structured and the drag force is reduced, while for  $\varepsilon = 6.498$  meV, a denser water layer forms around the nanotube, assisting the fluid-structure interaction and thus leading to a larger drag force. This tunability provides an alternative approach to engineer the fluid-structure interaction at the nanoscale, e.g., by applying an electrical or strain field [33,34].

#### IV. CONCLUSION

In summary, we conclude that at low speeds ( $u < 100$  m/s), the Stokes law  $C_D = CRe^{-1}$  gives a reasonable prediction for flow resistance around a carbon nanotube, while at a higher speed, the reduction of viscosity due to local heating significantly weakens the drag force and decreases the scaling parameter  $\alpha$  in  $C_D = CRe^\alpha$ . This effect cannot be captured by CFD. Moreover, we find that vibrational coupling between the fluid and structure facilitates mechanical energy transfer from the water flow into phonon modes of carbon nanotube. This excess kinetic energy further induces dramatic heating of the nanotube and water molecules around, and subsequently reduces the viscosity and drag force.

The results presented in this work have direct implications for the design of nanoscale devices, e.g., for the estimation of viscous damping on carbon nanotube resonators, nanofluidic sensors using flexural carbon nanotube arrays, and flow energy harvesters where mechanical energy can be transferred from the flow to nanostructures [5,6]. The vibrational energy transfer mechanism revealed here not only suggests limitations of the high-speed applications of nanostructure-based devices, but also implies efficient mechanical energy harvesting approaches as the kinetic and elastic energy of nanostructures can be channeled out. The latter ones can subsequently be converted into electricity through thermoelectric or piezoelectric devices. The tunable fluid-structure interaction through the geometry of carbon nanotubes and adhesive strength can further find broad applications in the field, such as nanoscale fluid cooling systems for these devices. A similar and interesting topic is vibration and instabilities induced by flow through carbon nanotubes, where flow-structure interactions can be informative for their applications in nanofluidics, nanofiltration, and desalination [35,36].

Another opportunity in understanding the nanoscale fluid-structure interaction resides in biological materials, especially protein materials in a solvent environment [37–39]. In these materials, nonbond interactions result in even lower vibrational

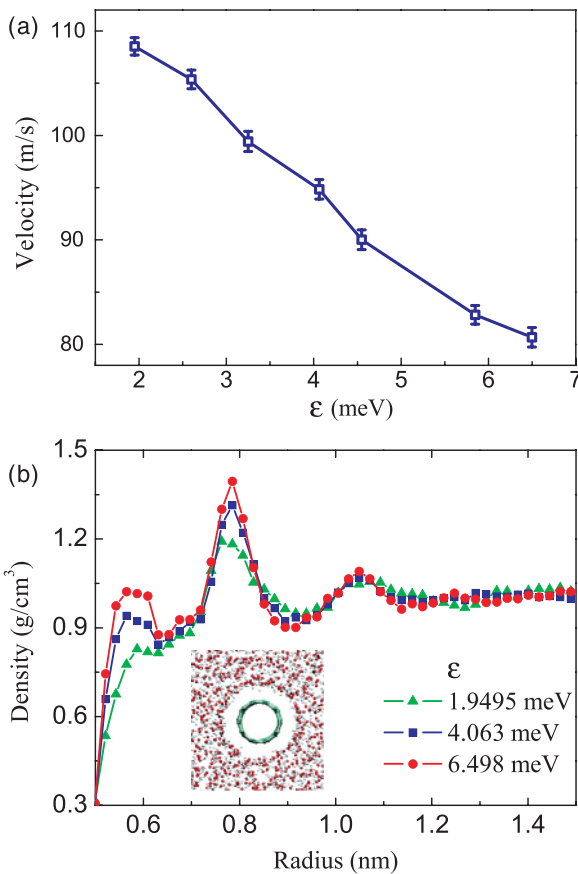


FIG. 6. (Color online) (a) Steady-state flow speed of water with different carbon-oxygen interactions but the same driving force. Here  $\sigma$  is kept as a constant as 0.319 nm, and  $\varepsilon$  is changed from 1.9495 to 6.498 meV, corresponding to contact angles from  $30^\circ$  to  $140^\circ$  (Table I). (b) The radial distribution function (RDF) of water molecules around the carbon nanotube for different  $\varepsilon$  values.

modes that can communicate more efficiently with flow in the physiological condition. Studies of these energetic processes at the atomistic level could benefit drug delivery technology, and help understand molecular mechanisms of diseases [40,41].

#### ACKNOWLEDGMENTS

We thank Dr. Yilun Liu for his help on the analysis of our simulation results. This work is supported by Tsinghua

University through the Key Talent Support Program, and the National Science Foundation of China through Grant No. 11002079 (Z.X.). Z.L. would like to acknowledge Small Grant 2010 from the engineering faculty of Monash University. L.S. appreciates support from the University of Sydney through the International Program Development Fund. Q.S.Z. acknowledges the National Science Foundation of China, Grants No. 10832005 and No. 10672089. The work is also supported by Shanghai Supercomputer Center of China.

- 
- [1] H. G. Craighead, *Science* **290**, 1532 (2000).
- [2] S. Ghosh, A. K. Sood, and N. Kumar, *Science* **299**, 1042 (2003).
- [3] J. Dornigac, A. Kalinowski, S. Erramilli, and P. Mohanty, *Phys. Rev. Lett.* **96**, 186105 (2006).
- [4] S. Sawano, T. Arie, and S. Akita, *Nano Lett.* **10**, 3395 (2010).
- [5] C. Chen and Z. Xu, *Nanoscale* **3**, 4383 (2011).
- [6] C. Chen, M. Ma, Z. Liu, Q. Zheng, and Z. Xu, *J. Appl. Phys.* **110**, 034320 (2011).
- [7] J. Happel, and H. Brenner, *Low Reynolds Number Hydrodynamics* (Martinus Nijhoff Publishers, The Hague, 1983).
- [8] M. Majumder, N. Chopra, R. Andrews, and B. J. Hinds, *Nature* **438**, 44 (2005).
- [9] Z. Xu, Q. Zheng, Q. Jiang, C.-C. Ma, Y. Zhao, G. Chen, H. Gao, and G. Ren, *Nanotechnology* **19**, 255705 (2008).
- [10] H. Lamb, *Hydrodynamics* (Cambridge University Press: Dover, New York, 1932).
- [11] J. H. Walther, T. Werder, R. L. Jaffe, and P. Koumoutsakos, *Phys. Rev. E* **69**, 062201 (2004).
- [12] D. M. Huang, C. Sendner, D. Horinek, R. R. Netz, and L. Bocquet, *Phys. Rev. Lett.* **101**, 226101 (2008).
- [13] J. A. Thomas and A. J. H. McGaughey, *Phys. Rev. Lett.* **102**, 184502 (2009).
- [14] S. Plimpton, *J. Comput. Phys.* **117**, 1 (1995).
- [15] P. G. Kusalik and I. M. Svishchev, *Science* **265**, 1219 (1994).
- [16] L. J. William, C. Jayaraman, D. M. Jeffry, W. I. Roger, and L. K. Michael, *J. Chem. Phys.* **79**, 926 (1983).
- [17] Y. Wu, H. L. Tepper, and G. A. Voth, *J. Chem. Phys.* **124**, 024503 (2006).
- [18] H. J. C. Berendsen, J. R. Grigera, and T. P. Straatsma, *J. Phys. Chem.* **91**, 6269 (1987).
- [19] M. A. Gonzalez and J. L. F. Abascal, *J. Chem. Phys.* **132**, 096101 (2010).
- [20] S. L. Mayo, B. D. Olafson, and W. A. Goddard III, *J. Phys. Chem.* **94**, 8897 (1990).
- [21] G. Gao, T. Çagin, and W. A. Goddard III, *Nanotechnology* **9**, 184 (1998).
- [22] T. Werder, J. H. Walther, R. L. Jaffe, T. Halicioglu, and P. Koumoutsakos, *J. Phys. Chem. B* **107**, 1345 (2003).
- [23] X. Chen, G. Cao, A. Han, V. K. Punyamurtula, L. Liu, P. J. Culligan, T. Kim, and Y. Qiao, *Nano Lett.* **8**, 2988 (2008).
- [24] J. K. Holt, H. G. Park, Y. M. Wang, M. Stadermann, A. B. Artyukhin, C. P. Grigoropoulos, A. Noy, and O. Bakajin, *Science* **312**, 1034 (2006).
- [25] M. Whitby and N. Quirke, *Nat. Nanotechnol.* **2**, 87 (2007).
- [26] J. A. Thomas and A. J. H. McGaughey, *Nano Lett.* **8**, 2788 (2008).
- [27] A. L. Tourmier and J. C. Smith, *Phys. Rev. Lett.* **91**, 208106 (2003).
- [28] *Physical Properties of Carbon Nanotubes*, edited by R. Saito, G. Dresselhaus, and M. S. Dresselhaus (Imperial College Press, London, 1998).
- [29] H. M. Lawler, D. Areshkin, J. W. Mintmire, and C. T. White, *Phys. Rev. B* **72**, 233403 (2005).
- [30] W. J. Weaver, S. P. Timoshenko, and D. H. Young, *Vibration Problems in Engineering* (Wiley-Interscience, Hoboken, NJ, 2001).
- [31] P. A. Greaney and J. C. Grossman, *Phys. Rev. Lett.* **98**, 125503 (2007).
- [32] P. A. Greaney G. Lani, G. Cicero, and J. C. Grossman, *Nano Lett.* **9**, 3699 (2009).
- [33] G. Manukyan, J. M. Oh, D. van den Ende, R. G. H. Lammertink, and F. Mugele, *Phys. Rev. Lett.* **106**, 014501 (2011).
- [34] W. Xiong, J. Z. Liu, M. Ma, Z. Xu, J. Sheridan, and Q. Zheng (unpublished).
- [35] J. Yoon, C. Q. Ru, and A. Mioduchowski, in *Proceedings of the International Conference on MEMS, NANO and Smart Systems, Banff, 2005*, edited by W. Badawy and W. Moussa (IEEE Computer Society, Los Alamitos, CA, 2005), p. 377.
- [36] T. A. Pascal, W. A. Goddard, and Y. Jung, *Proc. Natl. Acad. Sci. USA* **108**, 11794 (2011).
- [37] M. J. Buehler, and Y. C. Yung, *Nat. Mater.* **8**, 175 (2009).
- [38] Z. Xu, R. Paparcone, and M. J. Buehler, *Biophys. J.* **98**, 2053 (2010).
- [39] Z. Xu and M. J. Buehler, *Phys. Rev. E* **81**, 061910 (2010).
- [40] J. Lou and C. Zhu, *Proc. Natl. Acad. Sci. USA* **105**, 13847 (2008).
- [41] Z. Chen, J. Lou, C. Zhu, and K. Schulten, *Biophys. J.* **95**, 1303 (2008).